REPORT DOCUMENTATION PAGE

Form Approved OMB No. 0704-0188

1. REPORT DATE *(DD-MM-YYYY)*	2. REPORT TYPE	3. DATES COVERED *(From – To)*
28-06-2004	Final Report	1 August 2003 - 01-Aug-04

4. TITLE AND SUBTITLE

Modelling the main ionospheric trough across the Northern Hemisphere

5a. CONTRACT NUMBER
FA8655-03-1-3025

5b. GRANT NUMBER

5c. PROGRAM ELEMENT NUMBER

6. AUTHOR(S)

Dr. Cathryn Mitchell

5d. PROJECT NUMBER

5d. TASK NUMBER

5e. WORK UNIT NUMBER

7. PERFORMING ORGANIZATION NAME(S) AND ADDRESS(ES)

University of Bath
Univ. of Bath
Bath BA2 7AY
United Kingdom

8. PERFORMING ORGANIZATION REPORT NUMBER

N/A

9. SPONSORING/MONITORING AGENCY NAME(S) AND ADDRESS(ES)

EOARD
PSC 802 BOX 14
FPO 09499-0014

10. SPONSOR/MONITOR'S ACRONYM(S)

11. SPONSOR/MONITOR'S REPORT NUMBER(S)
SPC 03-3025

12. DISTRIBUTION/AVAILABILITY STATEMENT

Approved for public release; distribution is unlimited.

13. SUPPLEMENTARY NOTES

14. ABSTRACT

This report results from a contract tasking University of Bath as follows: The contractor will investigate disturbances in the Northern Hemisphere ionosphere using a Multi-instrument data analysis (MIDAS) imaging algorithm. This technique will be applied to existing data that has been previously collected by the contractor and other public sources. The final report will contain an analysis of these measurements.

20040920 085

15. SUBJECT TERMS
EOARD, Magnetosphere, Imaging, Ionosphere

16. SECURITY CLASSIFICATION OF:			17. LIMITATION OF ABSTRACT	18. NUMBER OF PAGES	19a. NAME OF RESPONSIBLE PERSON
a. REPORT	b. ABSTRACT	c. THIS PAGE			MICHAEL KJ MILLIGAN, Lt Col, USAF
UNCLAS	UNCLAS	UNCLAS	UL	28	19b. TELEPHONE NUMBER *(Include area code)* +44 (0)20 7514 4955

Standard Form 298 (Rev. 8/98)
Prescribed by ANSI Std. Z39-18

BEST AVAILABLE COPY

Report for USAF EOARD contract number FA8655-03-1-3025

Modelling the main ionospheric trough across the Northern Hemisphere

19 May 2004

Cathryn Mitchell, Department of Electronic and Electrical Engineering,
University of Bath, BA2 7AY, UK.

Project Summary

The aim of this work is to produce a real-time, measurement-driven model of the main trough in the ionosphere. The work applies the analysis and imaging techniques at the University of Bath to Global Positioning System (GPS) data and develops a method to use the ionospheric data recorded on a USAF instrument on-board the CHAMP satellite. The MIDAS (Multi-Instrument Data Analysis System) algorithm is used to invert the GPS data to produce movies of the ionospheric trough during selected periods during 2000 to 2002. The temporal and spatial resolution of these movies is sufficient to gain significant new information about the trough location, depth and dynamics. The results are compared with (a) the Paramaterized Ionospheric Model, (PIM) model and (b) data from the Langmuir Probe (LP) on the CHAMP satellite. The potential to use the LP observations as an input to a new Northern Hemisphere model of the trough is studied.

This work has applications in the following areas:

- *Forecasting ionospheric propagation at HF radio frequencies*
- *Improvements in mid-to-high latitude ionospheric models*
- *Locating ionospheric regions likely to cause scintillation, i.e. on the poleward trough wall*

1 Introduction

The Multi-Instrument Data Analysis System (MIDAS) is a global imaging system for the ionosphere and troposphere. MIDAS images of the ionosphere have been shown to reproduce the trough position and shape under both quiet and disturbed geomagnetic conditions (Meggs et al., 2004, Yin et al., 2004). In this report, MIDAS is used to provide a large database of trough images with a view to model testing and development. In addition, the detection of the trough using the *in-situ* USAF Langmuir probe on-board the German CHAMP satellite is investigated.

The overall aims are:
to test the PIM model and the LP against MIDAS
to produce an empirical 'parameter-driven' model of the trough from MIDAS
to demonstrate a measurement-driven trough model.

2 Method

The method for reconstructing images and movies of the ionosphere using MIDAS can be found in Mitchell and Spencer (2003). In this work, one-hour movies of the ionosphere over Europe were created from ground-based GPS data at selected periods during the current solar maximum. The image region covered longitudes 10°W to 40°E in steps of 2° and latitudes 30°N to 75°N in steps of 1°.

The analysis of the trough position in the movies was as follows. For the first frame of each one-hour movie a particular longitude was selected (0° or 30°E) and the TECs were calculated at latitudes between 40°N and 70°N. Each minima (turning point) in TEC was found and the one with the lowest value was selected.

3072 one-hour movies were produced from the year 2000 and 3336 movies were produced from the year 2001.

The presence and latitudinal location of the trough minimum for each image was recorded. These values were stored sequentially, one for each image. The value of latitude for each image was then considered in turn. If images from the adjacent two hours contained troughs that were greater than 5° and 10° apart in latitude from the one in question it was discarded. This reduces the likelihood of including anomalous features in the analysis, since the trough is a long-lived feature lasting throughout the night.

Once the trough had been identified in this manner, the following parameters were recorded:

- date
- universal time & local time
- latitude (geographic and geomagnetic)
- minimum TEC
- equatorward width & poleward width
- gradient on equatorward wall & gradient on poleward wall

In addition, the following magnetic parameters were recorded:

- the three hours planetary geomagnetic index, Kp
- the equatorial ring current, Dst
- the auroral electrojet index, Ae
- the polar cap index Pc
- interplanetary magnetic field components, IMF(y) & IMF(z)

3 Comparison with the Langmuir probe

The Langmuir probe (LP) on-board the CHAMP satellite records the ion density at the satellite altitude (around 350 km). Details about the instrument can be found in Cooke et al. (2003). In this work here it is of interest because depletions in the ion density are signatures of the trough.

Figures 3.1a to 3.8a show the MIDAS maps of the ionospheric vertical TEC (left) with the lowest TEC values in the trough marked in blue. The ion densities from the LP are also shown (right) and indications of the trough are found at the lowest values. In all cases the measurements from the two techniques are no more than half an hour apart in time. It can be seen that the trough is a rather large-scale ionospheric feature that is clearly detected in both the MIDAS images and the LP data.

Figure 3.9 makes a statistical comparison on this small sample from the year 2000. The MIDAS troughs have been taken from 0° longitude. It can be seen that the LP measurements and the MIDAS images are in good agreement about the trough position. Again, for 2001 (Figure 3.10) there is reasonable agreement, although there is some anomalous detection of the trough in three cases. These all occur on consecutive days in September. Appendix A shows that in each of these cases the LP is detecting a high-latitude trough that is not apparent in the MIDAS images. Nevertheless, in each of these cases the LP is also monitoring the main trough at a lower latitude. Appendix B shows the comparison between the LP and PIM.

These initial results indicate that the LP is a reliable instrument for detecting the trough. However, more extensive analysis of the LP data on its own would be required to use it in a routine manner for this task.

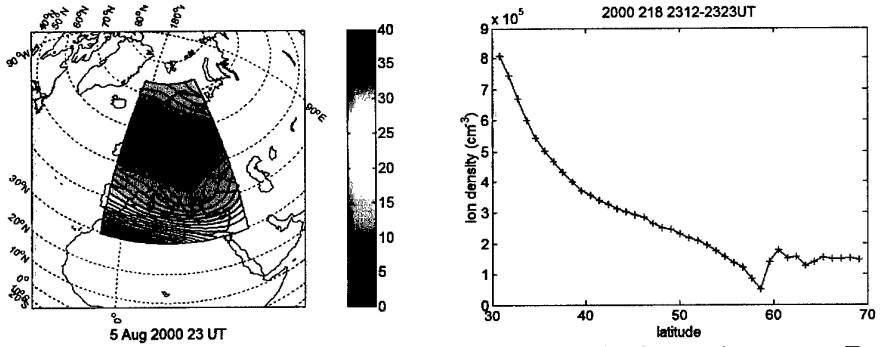

Figure 3.1a. MIDAS image of the vertical TEC across the ionosphere over Europe and b. ion density from the (southward) CHAMP satellite orbiting between 12° and 15° longitude.

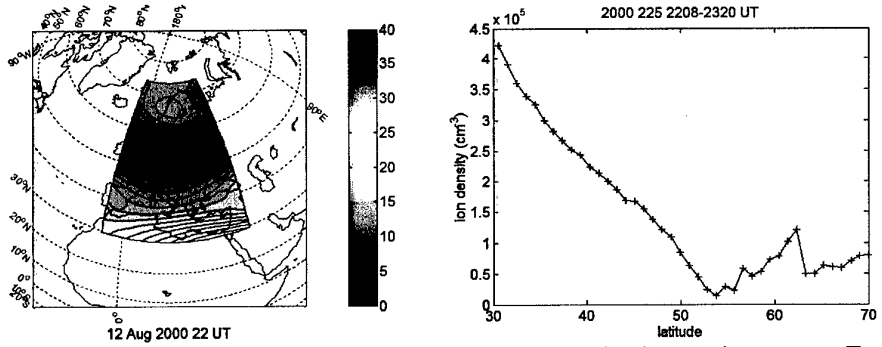

Figure 3.2a. MIDAS image of the vertical TEC across the ionosphere over Europe and b. ion density from the (southward) CHAMP satellite orbiting between 18° and 21° longitude.

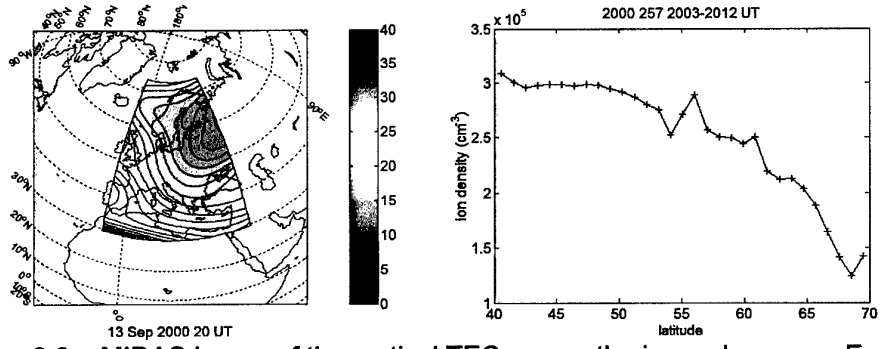

Figure 3.3a. MIDAS image of the vertical TEC across the ionosphere over Europe and b. ion density from the (southward) CHAMP satellite orbiting between 6° and 9° longitude.

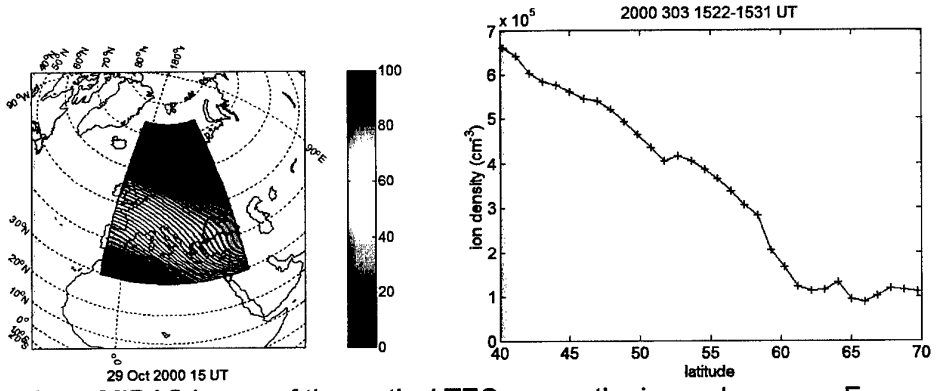

Figure 3.4a. MIDAS image of the vertical TEC across the ionosphere over Europe and b. ion density from the (southward) CHAMP satellite orbiting between 14° and 17° longitude.

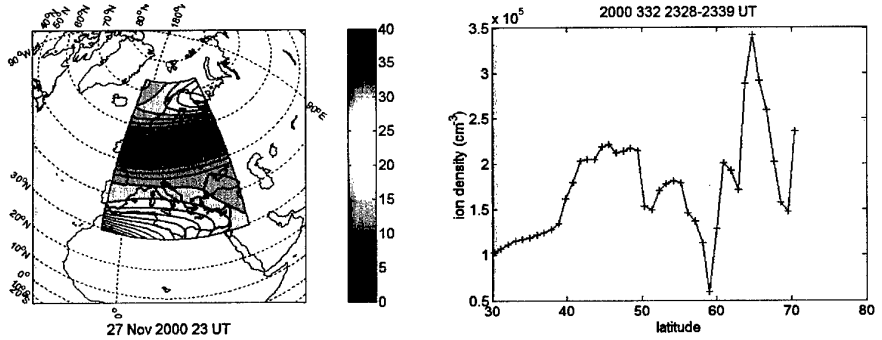

Figure 3.5a. MIDAS image of the vertical TEC across the ionosphere over Europe and b. ion density from the (northward) CHAMP satellite orbiting between 41° and 45° longitude.

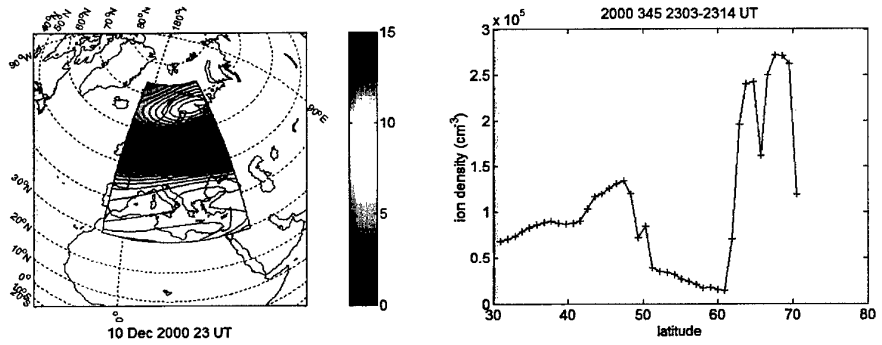

Figure 3.6a. MIDAS image of the vertical TEC across the ionosphere over Europe and b. ion density from the (northward) CHAMP satellite orbiting between 30° and 34° longitude.

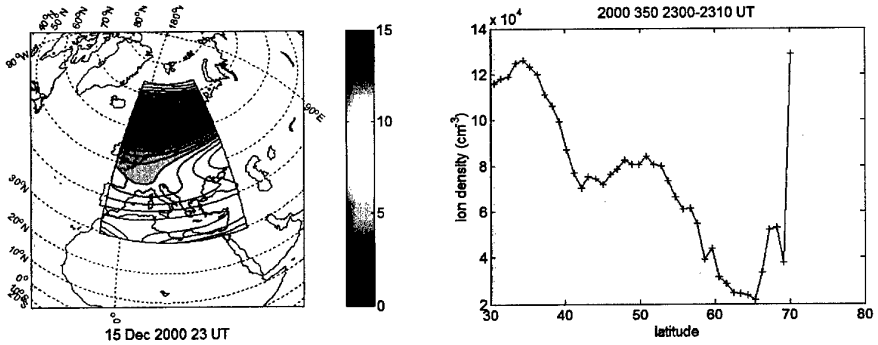

Figure 3.7a. MIDAS image of the vertical TEC across the ionosphere over Europe and b. ion density from the (northward) CHAMP satellite orbiting between 24° and 27° longitude.

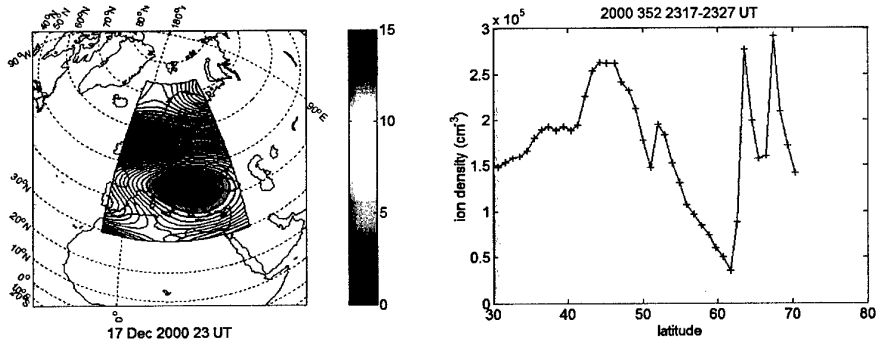

Figure 3.8a. MIDAS image of the vertical TEC across the ionosphere over Europe and b. ion density from the (northward) CHAMP satellite orbiting between 17° and 20° longitude.

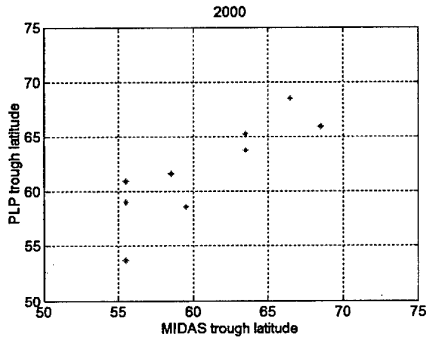

Figure 3.9. Geographic latitude of the LP trough and the MIDAS trough for the year 2000 (standard deviation 2.77°, maximum difference 5.41°)

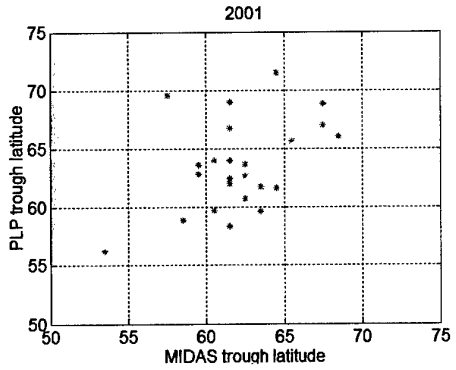

Figure 3.10. Geographic latitude of the LP trough and the MIDAS trough for year 2001 (standard deviation 3.98°, maximum difference 12.10°). The largest differences occur on days 250, 251 and 252 (see Appendix A).

4 Forecasting the trough location

Having established that the LP can detect the position of the main trough, it is now of interest to try forecasting the trough position making use of the current measurement.

Since the LP is currently only on one low-Earth-orbit satellite it cannot make measurements of the ionosphere over Europe at each hour. For this reason only the MIDAS troughs have been used here for the forecasting. However, it should be noted that this could be extended to using the LP.

The initial procedure was to find those measurements of the trough position that were consecutive and to use simple one-hour persistence on the geomagnetic latitude of the minimum as a forecast. The results are divided into two graphs Figure 4.1a and 4.1b – one for evening (16-24 UT) and the other for morning (00 to 06 UT). This simple method gives a reasonable forecast of trough position. Large errors are not due to an extreme movement of the trough, rather they are the result of the detection algorithm in the original determination of the troughs moving between the main trough and other high-latitude depletions in the ionisation.

Figure 4.2 has the calculated movement of the trough per hour from Section 5 (1.13° per hour) factored into the forecast of the latitude. This improves the pre-midnight results by removing the bias from the southward movement of the trough during the evening.

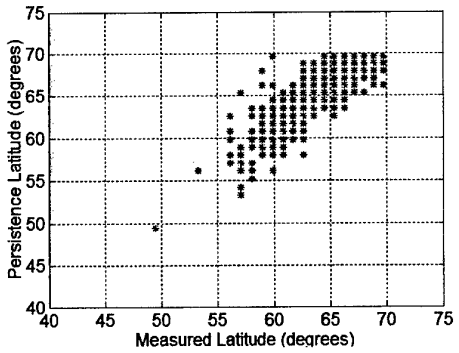

Figure 4.1a. Geomagnetic latitude of the trough (before midnight) using one-hour persistence and the actual (measured) trough position. This gives a standard deviation of 2.49° and a maximum difference of 9.80°.

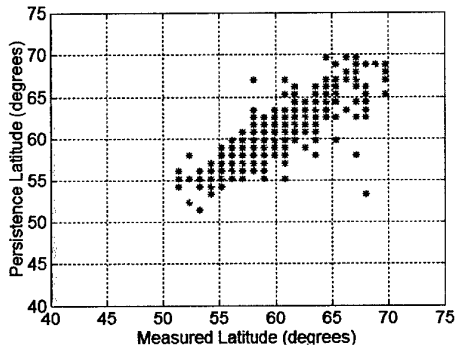

Figure 4.1b. Geomagnetic latitude of the trough (after midnight) using one-hour persistence and the actual (measured) trough position. This gives a standard deviation of 2.05° and a maximum of 14.71°.

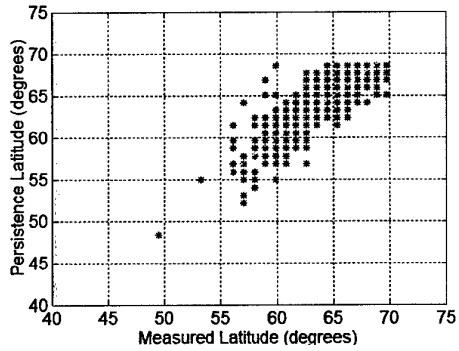

Figure 4.2. Geomagnetic latitude of the trough (before midnight) using one-hour persistence with an average movement of 1.13 degrees south per hour and the actual (measured) trough position. This gives a standard deviation of 2.11° and a maximum difference of 8.71° (compare with Figure 4.1a).

5 Modelling the trough location

The next stage relates to the stand-alone model of the trough, based on conventionally used parameters.

The trough position was defined in terms of the latitude of the minimum. The calculation of the minimum is explained in Section 3. Other factors correlating with the trough location were identified and characterised by measurement or index. These factors were either related to time or to geomagnetic activity. The temporal dependence was contained within Universal Time (UT), Local Time (LT) and daynumber. The reason for including both UT and LT was to account for changes in the trough behaviour with longitude. For this reason LT can really be considered to be a spatial rather than a temporal term.

A day number term was created to accommodate seasonal variations. It is defined as

$$dn = (\text{daynumber} - 157)^2 \qquad (5.1)$$

The geomagnetic effects were contained within the indices Kp and Dst. Other indices (PC and Ae) were found to offer no improvement in the determination of the trough position.

Table 5.1 shows the parameters calculated for a linear model fit of the year 2000 data. Column 1 simply names the model (e.g. A) and column 2 defines the co-ordinates (geographic, GG or geomagnetic, GM). The following six columns show the calculated parameters for a linear model. The final two columns of Table 5.1 denote the standard deviation and the maximum errors.

The first four models (A-D) were formed/tested for data collected at a single longitude (0°). Models G and H were for multiple longitudes (0° and 30°E).

Taking an example from the results table, F is a least-squares linear model for the geographic latitude of the trough from a combination of local time, Kp, Dst and day number (dn),

$$\Delta = 66.5 + 1.2LT - 0.9Kp + 0.03Dst - 0.23dn \qquad (5.2)$$

where LT was defined as 24-local time (hours).

The results relate mainly to the pre-midnight sector unless otherwise stated. Figures 5.1 to 5.11 show the measured trough position (x-axis) against the calculated trough position for the various models of Table 5.1. If all of the points lay on the line shown in white the model would be ideal.

It can be seen that the use of geomagnetic indices (Figure 5.2 and 5.3) is important for modelling the trough position. This is entirely expected. However, Figure 5.4 shows a new result – the introduction of the seasonal term is very important, reducing the standard deviation to 2.7° and the maximum to 5.7°.

Figure 5.6 and 5.7 show the location of the trough from the PIM model. It is interesting to see the absence of any bias in the model, although the determination of

the position of the trough is not as accurate (standard deviation 3.7°) as some other methods.

Figure 5.8 shows results where geomagnetic co-ordinates were used, with the trough modelled in terms of local time, geomagnetic activity (Kp and Dst) and daynumber. We now move to modelling the trough at multiple longitudes. Figure 5.9 includes data from 0 and 30°E and it can be seen that the errors have increased. However, this is because the trough does not exactly follow lines of geomagnetic latitude and the inclusion of the term UT to account for this (Figure 5.10 and 5.11) reduces the errors again.

Model H provides a generalised model of the LT evening geomagnetic latitude of the trough.

$$\Delta = 64.9 + 3.4LT - 0.6Kp + 0.03Dst - 2.2UT - 0.18dn \qquad (5.3)$$

	GG or GM	Constant	LT	Kp	Dst	Seasonal	UT	Std dev	Max
A	GG	58.34	1.14					**3.81**	**14.12**
B	GG	60.60	1.18	-0.88				**3.59**	**10.09**
C	GG	60.37	1.18	-0.61	0.03			**3.52**	**9.32**
D	GG	64.80	1.34	-0.98	0.04	-0.26		**2.66**	**7.71**
D2	GG	64.77	1.33	-0.98	0.03	-0.25		**2.66**	**7.66**
E PIM	GG							**3.75**	**14.50**
E2 PIM	GG							**3.69**	**11.50**
F	GM	66.47	1.21	-0.89	0.03	-0.23		**2.41**	**7.05**
G 0 & 30°	GM	63.15	1.31	-0.90	0.00	-0.18		**3.58**	**21.43**
H	GM	64.88	3.44	-0.60	0.03	-0.18	-2.22	**2.74**	**18.99**
H2	GM	65.18	3.37	-0.66	0.03	-0.19	-2.18	**2.59**	**11.45**

Table 5.1. The parameters calculated to model the trough position during 2000 (pre-midnight) for various linear models. A local time, B local time and Kp, C local time, Kp, Dst and season, D2 local time, Kp, Dst and season (restricted dataset), E PIM, E2 PIM restricted dataset), F As for D but geomagnetic, G As for F but with 0 and 30 longitude, H local time, Kp, Dst, season and UT, restricted dataset.

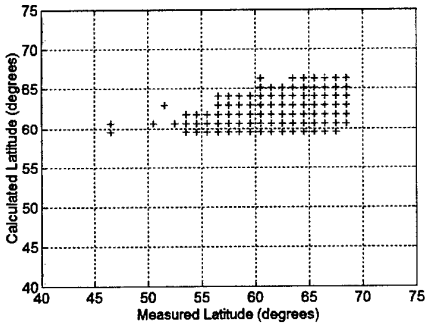

Figure 5.1. Measured and calculated trough position for Model A of Table 5.1.

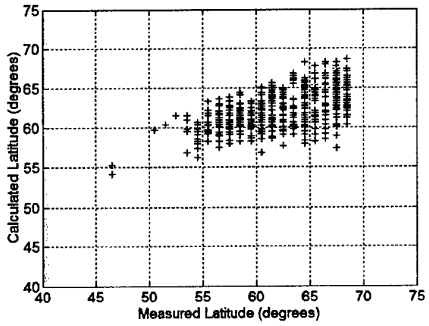

Figure 5.2. Measured and calculated trough position for Model B of Table 5.1.

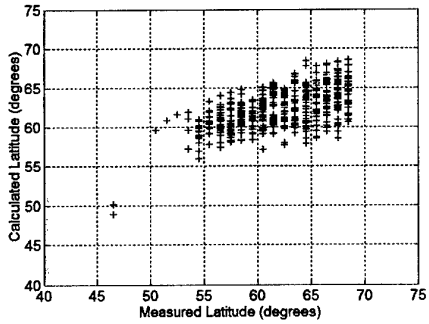

Figure 5.3. Measured and calculated trough position for Model C of Table 5.1.

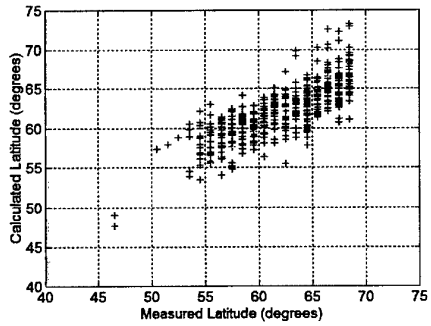

Figure 5.4. Measured and calculated trough position for Model D of Table 5.1.

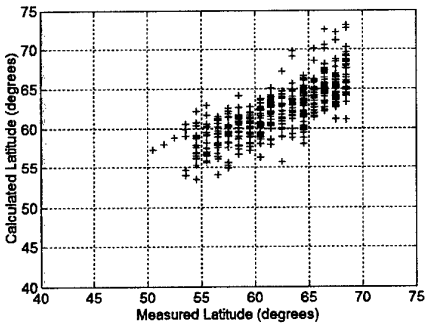

Figure 5.5. Measured and calculated trough position for Model D2 of Table 5.1. (without points below 49 geographic)

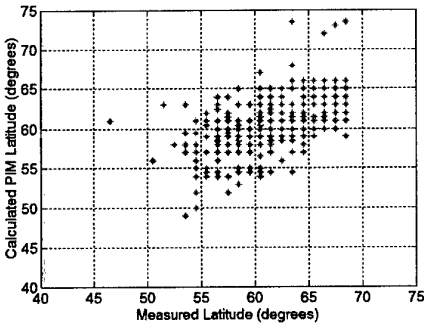

Figure 5.6. Measured and calculated trough position for PIM (E) of Table 5.1.

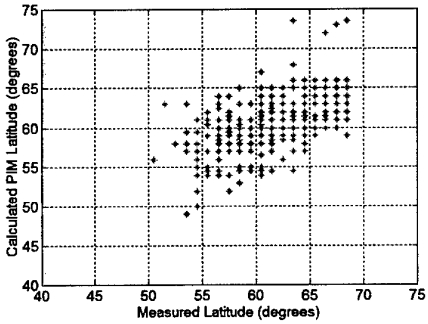

Figure 5.7. Measured and calculated trough position for PIM (E2) of Table 5.1.

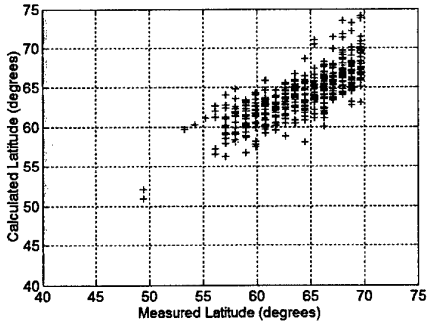

Figure 5.8. Measured and calculated trough position for Model F of Table 5.1

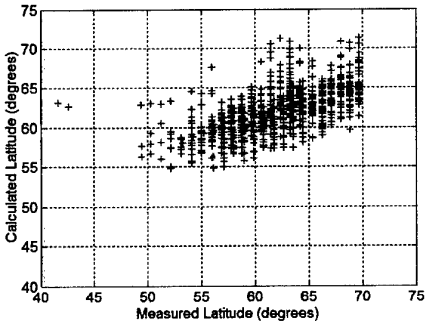

Figure 5.9. Measured and calculated trough position for Model G of Table 5.1.

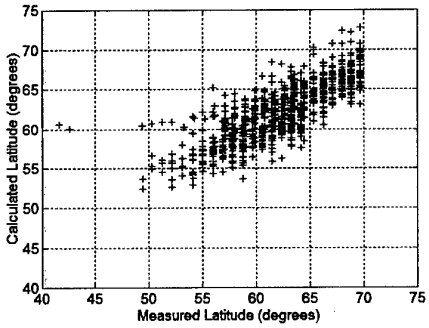

Figure 5.10. Measured and calculated trough position for Model H of Table 5.1.

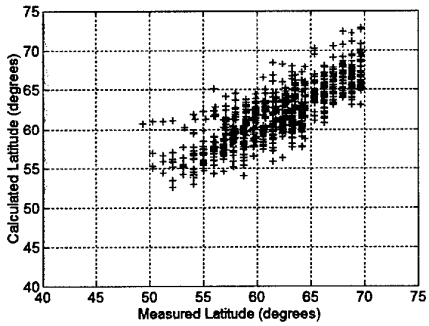

Figure 5.11. Measured and calculated trough position for Model H2 of Table 5.1.

6 Modelling the minimum TEC

The same procedure to calculate the trough latitude was now applied to model the value of the trough minimum TEC. The least and most successful results are shown in Table 6.1 (A and D) and Figure 6.1 and 6.2. Equation 6.1 shows the optimal values for Model D, in TECU,

$$\text{minTEC} = 15.1 + 0.97\,LT - 0.4\,Kp + 0.03\,Dst - 0.41dn \qquad (6.1)$$

Since all of the data are at solar maximum no attempt has been made here to include the solar activity index in the model. Nevertheless, it is recognised that sunspot number will be important to factor in when using the model at other solar activity levels.

The PIM model results are also shown for comparison in Table 6.1 (E2) and Figure 6.3.

	Constant	LT	Kp	Dst	Seasonal	Std dev	Max
A	7.68	0.65				6.39	21.92
D	15.11	0.97	-0.42	0.04	-0.41	4.34	15.31
E2						4.87	28.38

Table 6.1. The parameters calculated to model the trough minimum TEC (pre-midnight) D2 local time, Kp, Dst and season (restricted dataset).

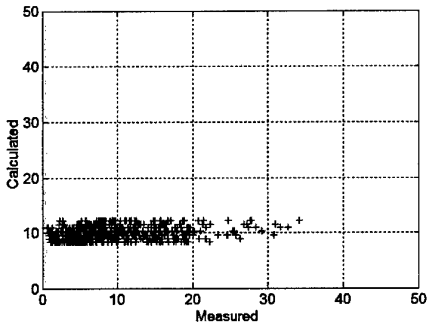

Figure 6.1. Measured and calculated trough minimum TEC (TECU) for Model A of Table 6.1 (year 2000).

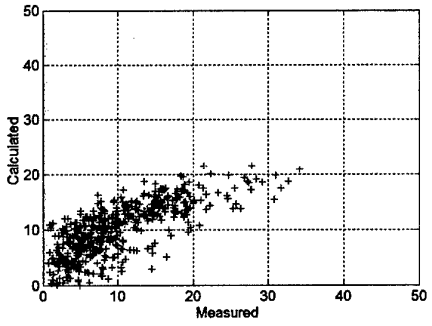

Figure 6.2. Measured and calculated trough minimum TEC (TECU) for Model D of Table 6.2 (year 2000).

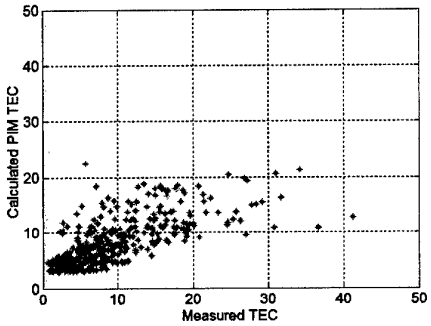

Figure 6.3. Measured and calculated trough minimum TEC for PIM (E2) of Table 6.2 (year 2000).

7 Testing the models on Year 2001 data

MIDAS images from year 2001 were used to test the models. The parameters from Model F of Table 7.1 were used to predict the trough minimum latitude using Kp, LT, Dst and day number. Figure 7.1 shows the measured latitude plotted against the predicted latitude. The standard deviation is 3.36° and the maximum error 15.14°.

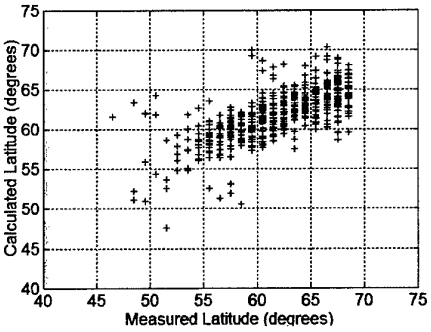

Figure 7.1. Measured and calculated geomagnetic trough latitude for YEAR 2001 for Model F of Table 7.1. Errors are standard deviation 3.36° and maximum 15.14°.

In order to make an evaluation of the model F, the PIM model is tested against the same database of images. The results are shown in Figure 7.2. The standard deviation is 4.98° and the maximum error 21°. There are clearly a small number of cases where it has not been possible to model the trough position during 2001.

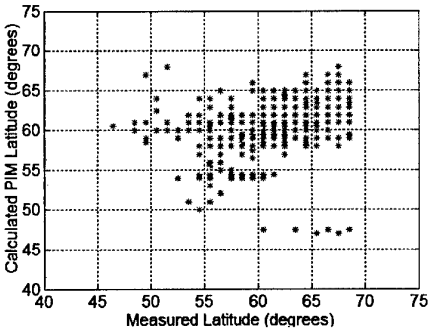

Figure 7.2. Measured and calculated trough position for YEAR 2001 for PIM. Errors are 4.98° (standard deviation) and 21° (maximum).

8 Other features of the trough

Characteristics of the trough other than its position were also calculated from the 2000 data. Appendix C shows the results of modelling these using the parameters of Kp, LT, Dst and day number. Mean and median values for certain trough parameters are given in Table 8.1. These can be used to create a stand-alone model of the trough.

The trough features were defined as follows. Feature (1), the pole width, is the difference in degrees geographic latitude between the trough minimum and the steepest gradient over 1° on the poleward wall. Feature (2), the equator width, is the difference in degrees geographic latitude between the trough minimum and the steepest gradient over 1° on the equatorward wall. Feature (3), the pole increase, is the percentage increase in TEC between the TEC at the trough minimum and the TEC at that point (1) on the poleward wall. Feature (4), the equator increase, is the percentage increase in TEC between the TEC at the trough minimum and the TEC at that point (2) on the equatorward wall. Feature (5), the pole gradient, is the percentage increase in TEC over the steepest 1° on the poleward wall (i.e. at position 1). Feature (6), the equator gradient, is the percentage increase in TEC over the steepest 1° on the equatorward wall (i.e. at position 2)

Feature	Mean	Median
1. Pole width	6.1°	6.0°
2. Equator width	6.4°	6.0°
3. Pole increase	58%	59%
4 Equator increase	63%	65%
5. Pole gradient	9%	10%
6. Equator gradient	8%	10%

Table 8.1. Mean and median values for trough features.

These values, together with a model of the trough position and minimum TEC from Sections 5 and 6, could be used to make a stand-alone model of the trough for incorporation into an empirical model such as IRI.

9 Summary

The overall aims of the project were:

- to test the PIM model and the LP against MIDAS
- to produce an empirical 'parameter-driven' model of the trough from MIDAS
- to demonstrate a measurement-driven trough model.

The findings of the report were as follows.

The LP was able to identify the trough to within 2.8° (std dev) on the 2000 data without systematic biases. On the 2001 data the results were skewed by anomalous measurements during early September. These seemed to relate to the presence of a secondary trough at high latitude observed in the LP data.

The PIM model was able to reproduce the MIDAS trough location without systematic biases on both 2000 and 2001 data (standard deviations 3.7°, 4.2° respectively).

An empirical model of the trough developed on Year 2000 data, working in terms of local time, universal time, Kp, Dst and day number gave an overall std dev of 2.6°. On year 2001 the standard deviation was 3.5°.

A real-time one-hour-ahead forecast model of the trough gave a standard deviation of 2.1°.

The PIM model gave a standard deviation of 4.9 TECU on the determination of the TEC at the trough minimum. The empirical model gave a standard deviation of 4.2 TECU. It should be noted that for general use the minimum TEC should be scaled appropriately by the solar activity index, since these results relate to solar maximum.

Averages of other trough features were found and have been stated so that a model of the trough can be created from the results of this report.

References

Bilitza, D., International Reference Ionosphere 1990, National Space Science Data Center/World Data Center A for Rockets and Satellites 90-22, 1990.
Cooke, D., H.Luehr, N. Jakowski, In situ plasma observation at 400 km on the CHAMP satellite, Geophysical Research
Abstract, Vol 5, 13004, 2003.
Daniell, R.E., Parameterized real-time ionospheric specification model: PRISM Version 1.0, Phillips Laboratory Technical Report, PL-TR-91-2299, Hanscom AFB, MA 01731, USA, 1991.
Meggs R W, C N Mitchell and V Howells, 'Simultaneous observations of the main trough using the EISCAT radar and GPS imaging', 'Annales Geophysicae, (2004, in press)
Mitchell C N and Paul S J Spencer, A three dimensional time-dependent algorithm for ionospheric imaging, Ann. Geophysicae, 2003.
Yin, P, C N Mitchell, P S J Sencer and J Foster, GRL, 2004, (in press).

Acknowledgements

The author of this report is very grateful for:

- the use of the PIM model (Daniell, 1991)
- the use of GPS data from the IGS network
- the Langmuir probe data from CHAMP (David Cooke, AFRL)

Appendix A. MIDAS and LP troughs from 2001

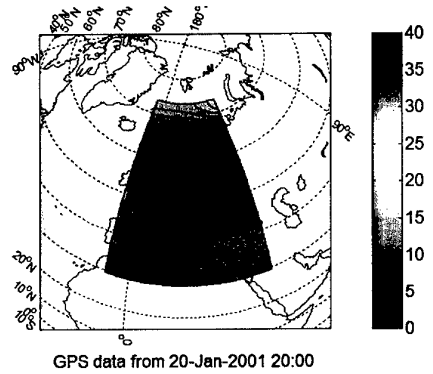

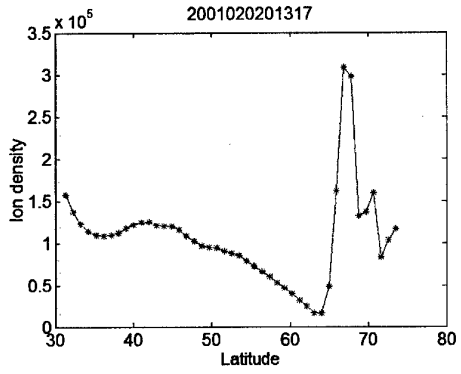

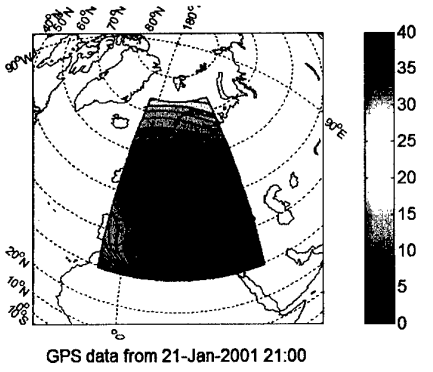

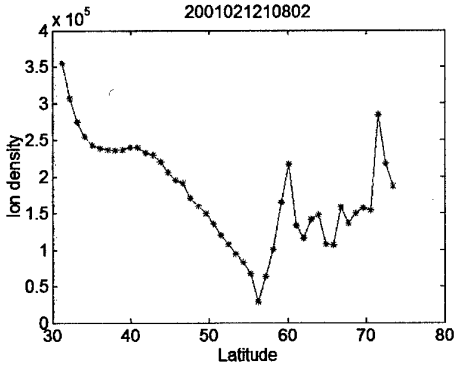

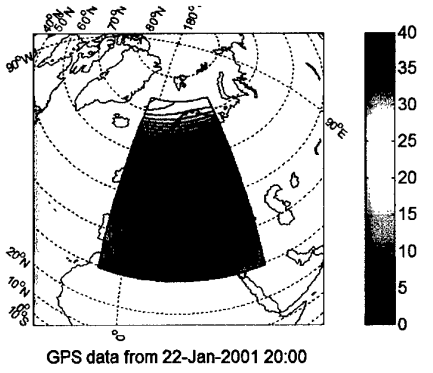

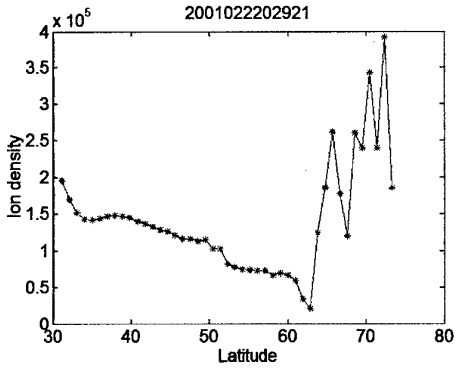

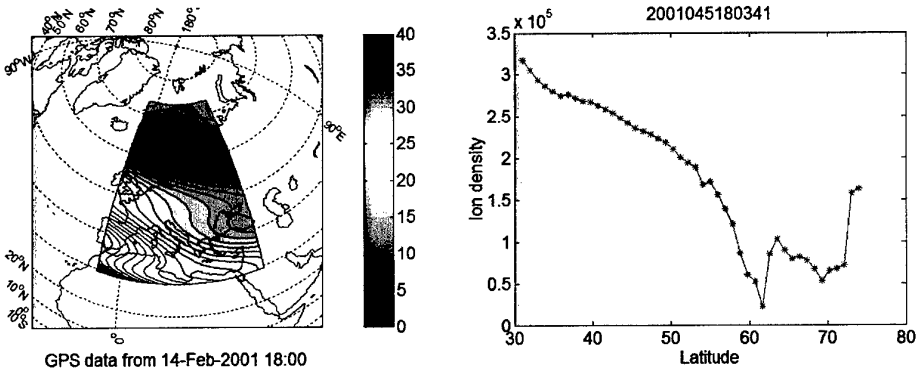

GPS data from 14-Feb-2001 18:00

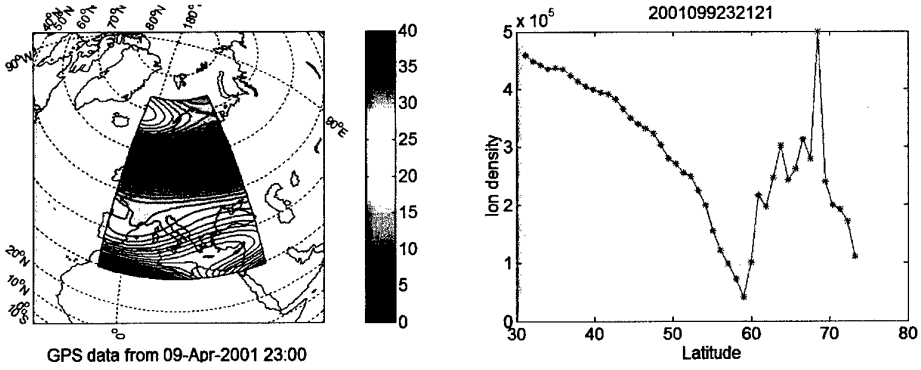

GPS data from 09-Apr-2001 23:00

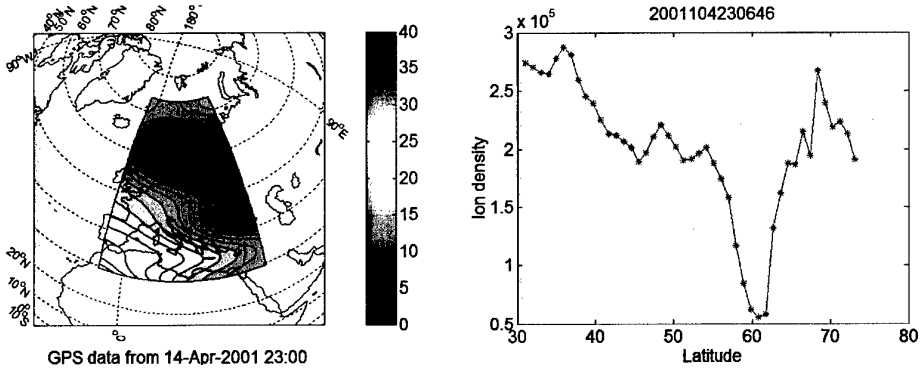

GPS data from 14-Apr-2001 23:00

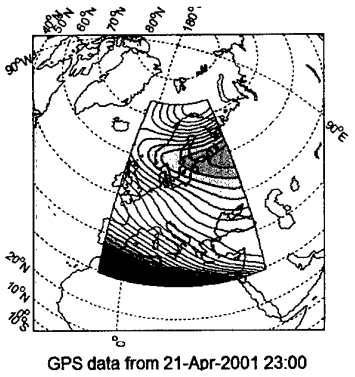

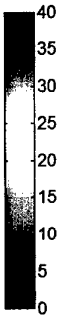

GPS data from 21-Apr-2001 23:00

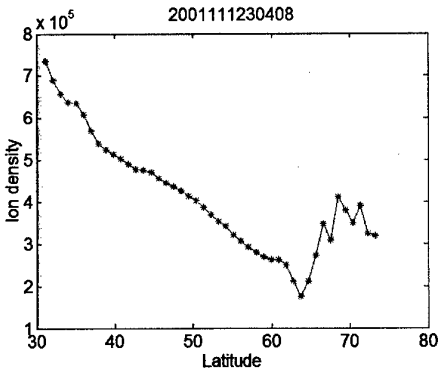

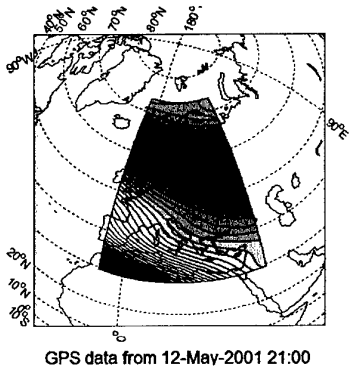

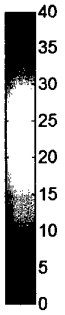

GPS data from 12-May-2001 21:00

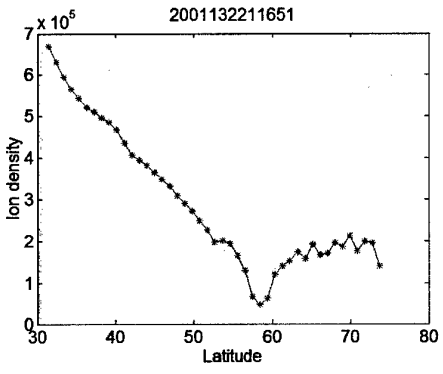

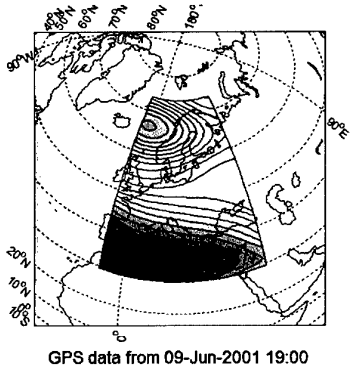

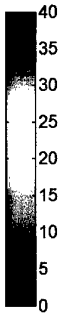

GPS data from 09-Jun-2001 19:00

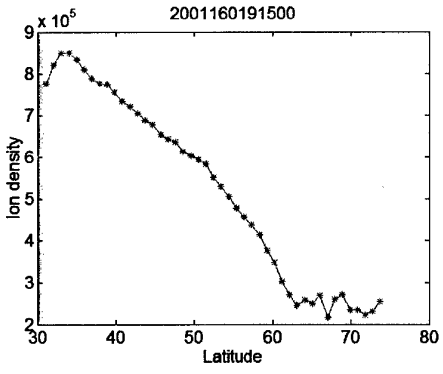

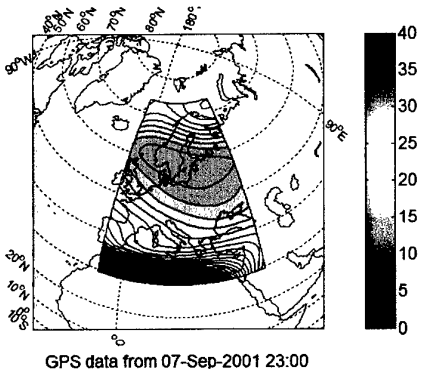

GPS data from 07-Sep-2001 23:00

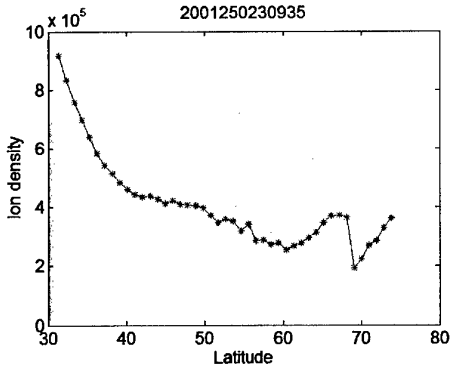

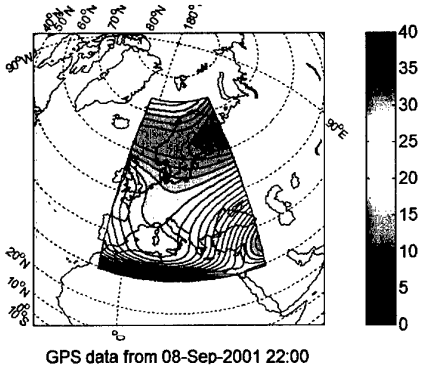

GPS data from 08-Sep-2001 22:00

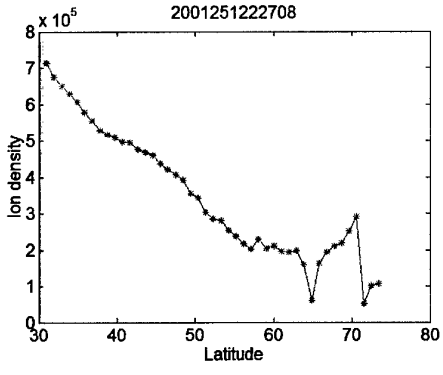

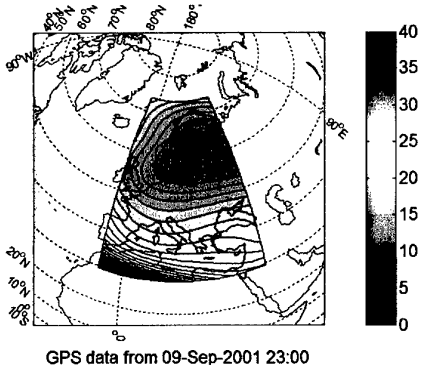

GPS data from 09-Sep-2001 23:00

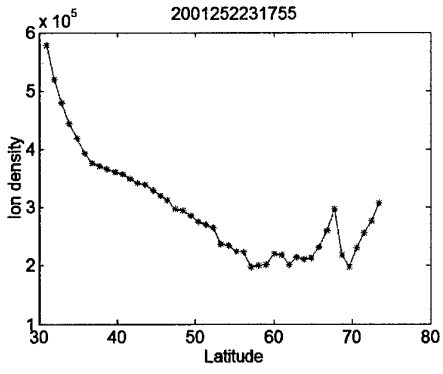

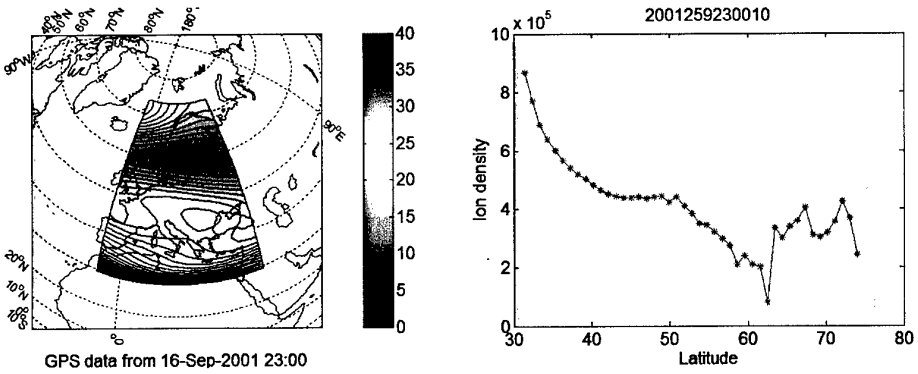
2001259230010
x 10^5
Ion density
Latitude
GPS data from 16-Sep-2001 23:00

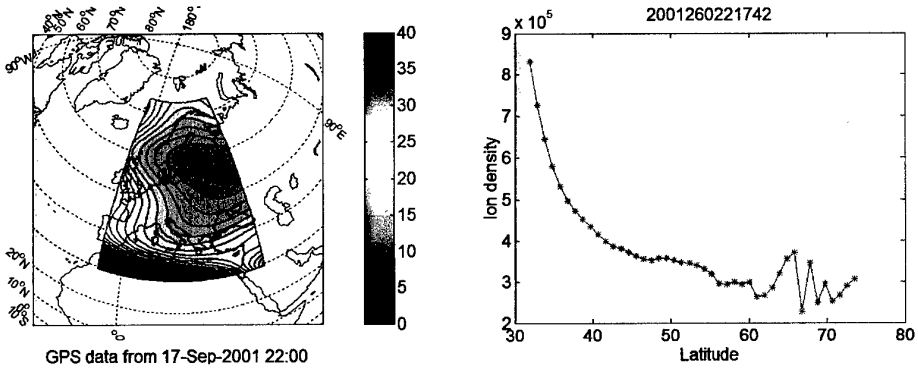
2001260221742
x 10^5
Ion density
Latitude
GPS data from 17-Sep-2001 22:00

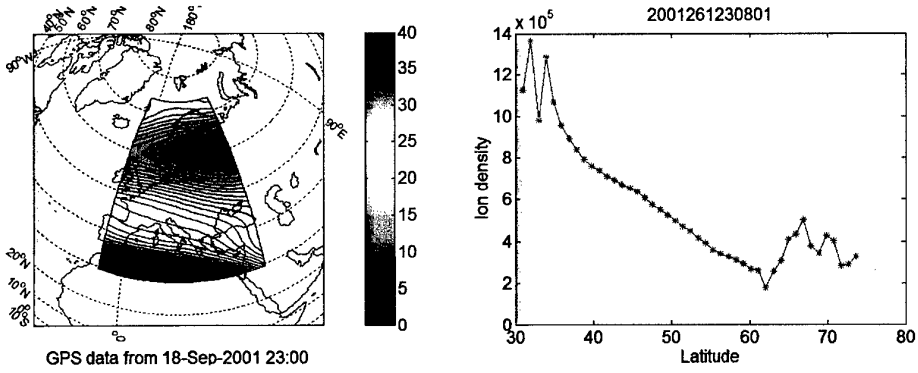
2001261230801
x 10^5
Ion density
Latitude
GPS data from 18-Sep-2001 23:00

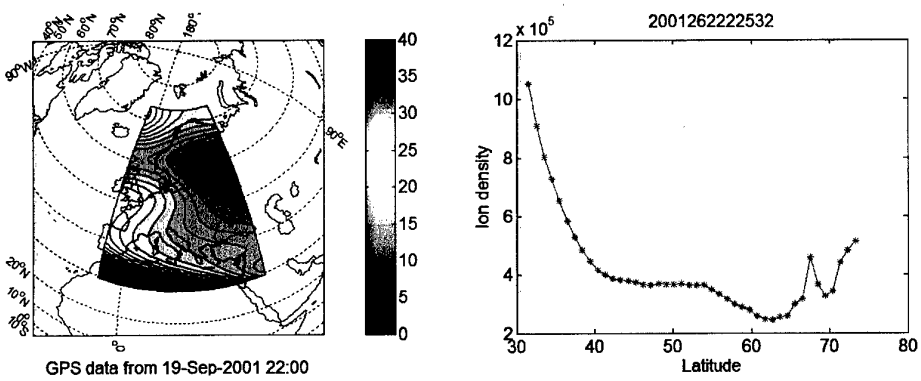

GPS data from 19-Sep-2001 22:00

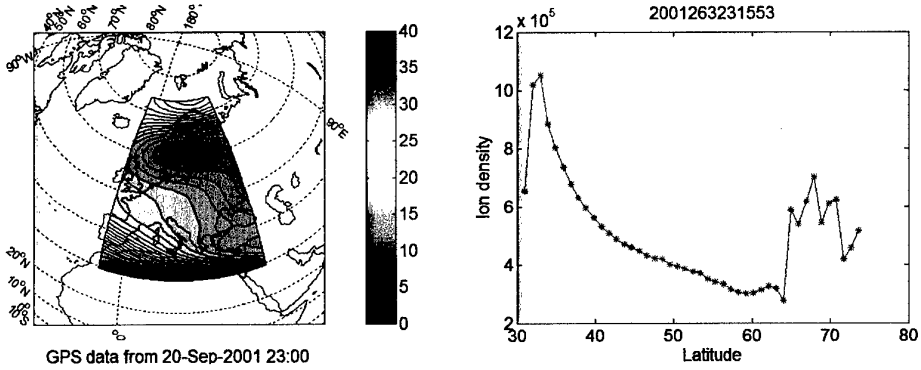

GPS data from 20-Sep-2001 23:00

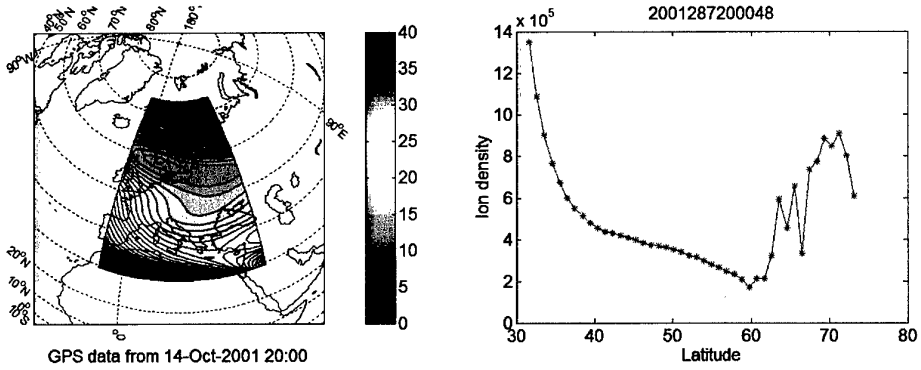

GPS data from 14-Oct-2001 20:00

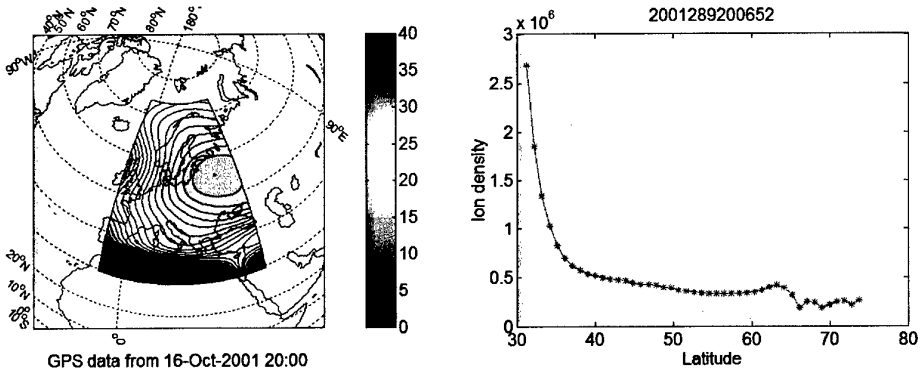
2001289200652
x 10^6
Ion density
Latitude
GPS data from 16-Oct-2001 20:00

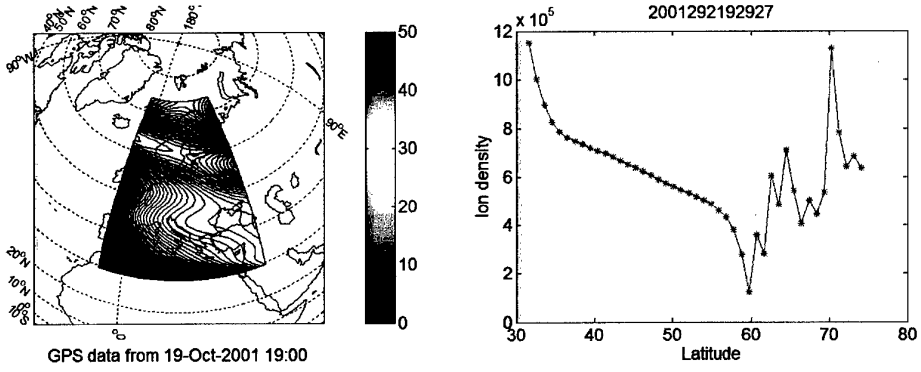
2001292192927
x 10^5
Ion density
Latitude
GPS data from 19-Oct-2001 19:00

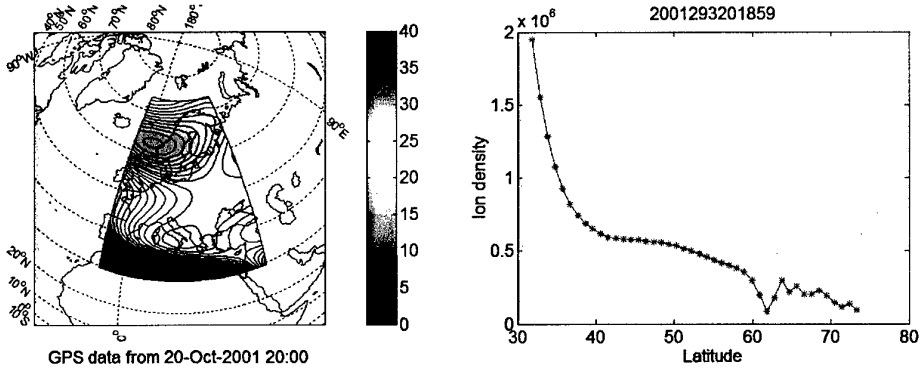
2001293201859
x 10^6
Ion density
Latitude
GPS data from 20-Oct-2001 20:00

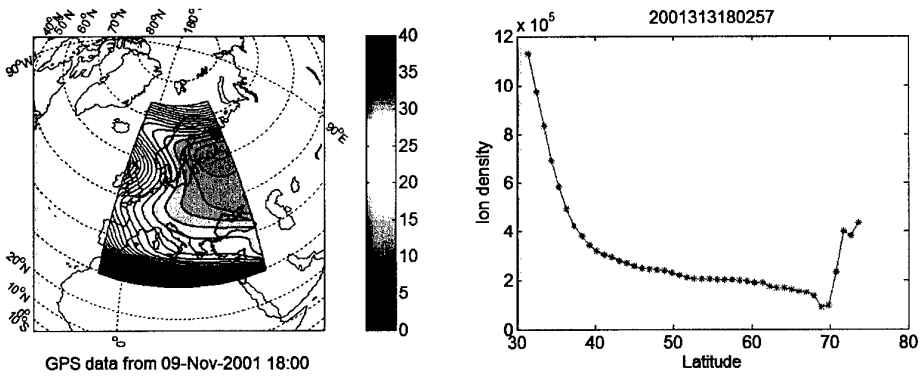
2001313180257
x 10^5
Ion density
Latitude
GPS data from 09-Nov-2001 18:00

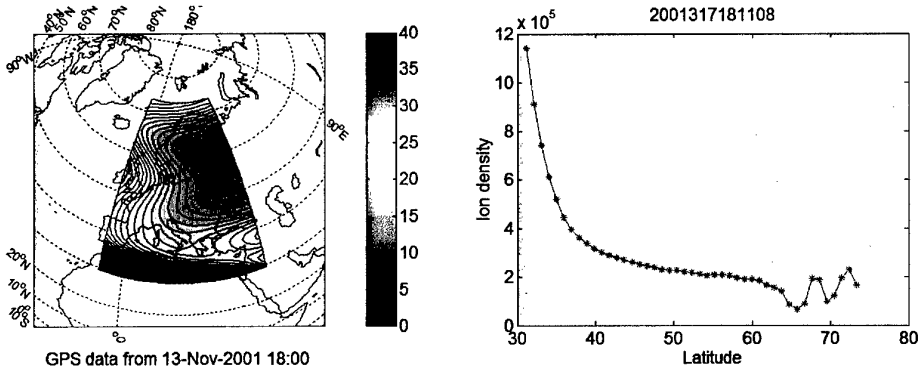
2001317181108
x 10^5
Ion density
Latitude
GPS data from 13-Nov-2001 18:00

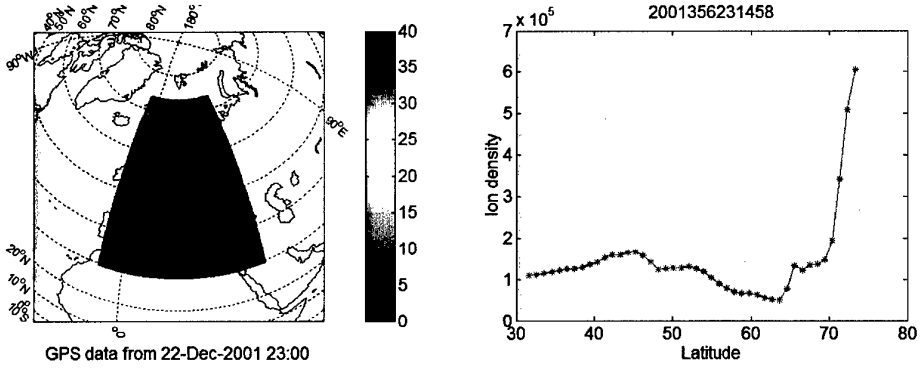
2001356231458
x 10^5
Ion density
Latitude
GPS data from 22-Dec-2001 23:00

Appendix B – Comparison between the LP and the PIM troughs

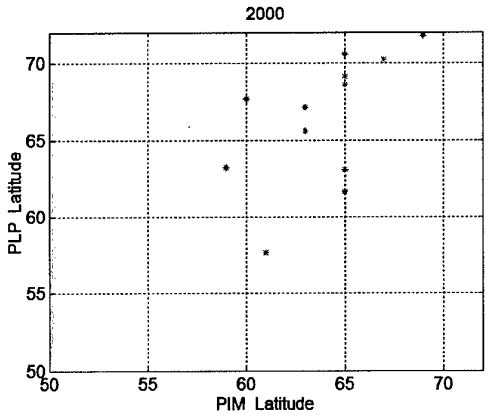

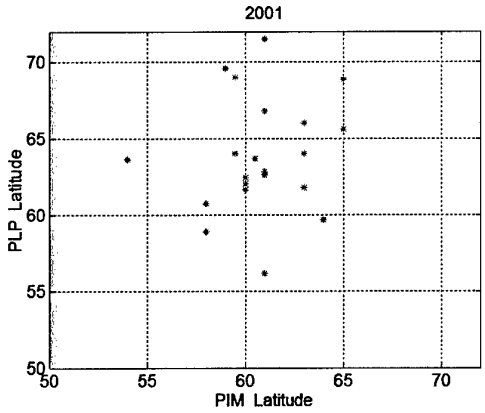

Appendix C - Other features relating to Section 8.

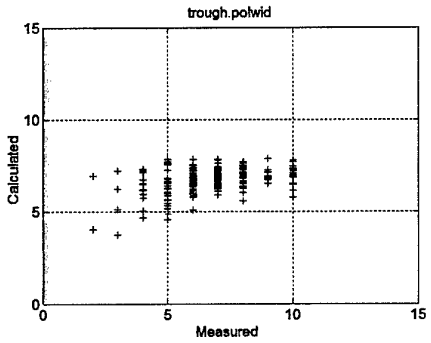

Figure B1

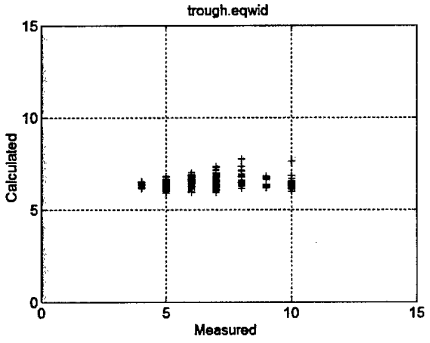

Figure B2

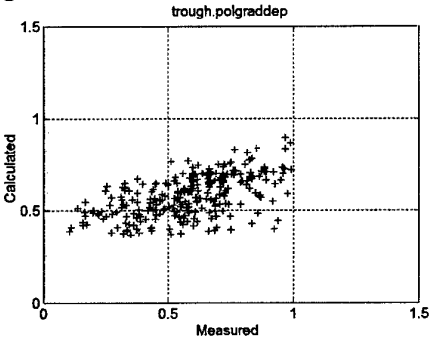

Figure B3

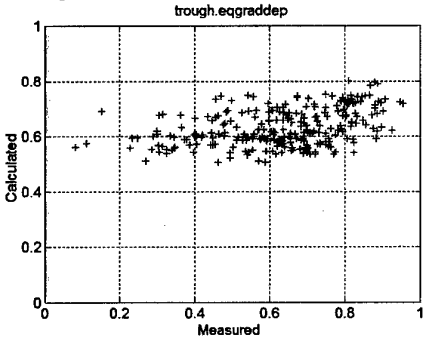

Figure B4

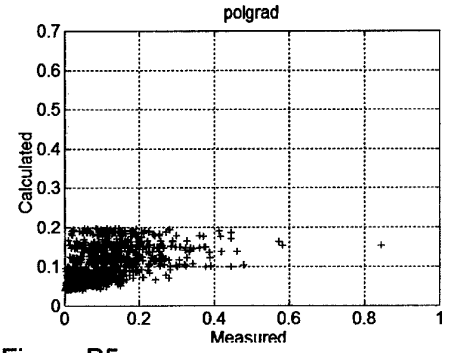

Figure B5

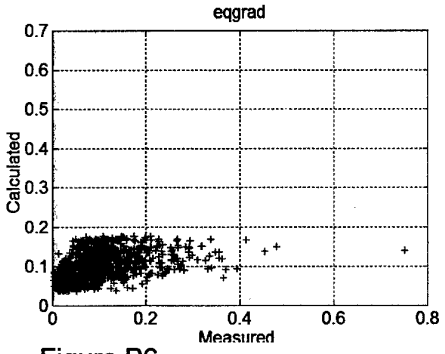

Figure B6